The Recombination Velocity at III-V Compound Heterojunctions with Applications to $Al_xGa_{1-x}As$-$GaAs_{1-y}Sb_y$ Solar Cells

金 正 淳
(Jung Soon Kim)

4. Strained and Strain-Free Lattice Mismatch

When heteroepitaxial layers are grown, two typer of defects [35, 36, 37] can usually be observed because of differences in the lattice constants and thermal expansion coefficients (see Fig. 15) In this chapter, the resulting bending[38] of the wafer and lattice defects introduced during growth (stacking faults) [35] are neglected. Attention is focused only on methods for obtaining the relative lattice mismatch between the heteroepitaxial layer and the substrate.

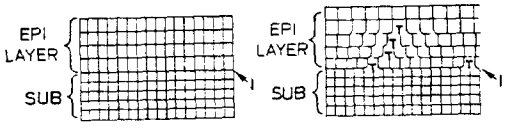

a. Elastic latticedeformation b. Misfit dislocations

Fig. 15. Defects at heterojunction interfaces. "I" indicates the epitaxial layer-substrate interface.

If there are no misfit dislocations at the heterojunction interface, the lattice mismatch is reli ved by elastic lattice deformation of the epitaxial layer, caused by stress at the interface, in which the spacing of the lattice planes normal to the growth surface does not change, but the spacing of the lattice planes parallel to the growth surface expands or contracts. In other words, the lattice constant of the epitaxial layer becomes uniform along the growth direction and much of the elastic strain resulting from the lattice mismatch remains in the layer. It has been reported [36, 37, 39, 40, 41] that in cubic and zincblende III-V compounds, the lattice of the epitaxial layer can be "tetragonally" deformed on (100) substrate orientations but "rhombohedrally" deformed on (111) substrate orientations.

When the lattice mismatch cannot be relieved by elastic lattice deformation, however, a misfit dislocation array (unidirectional or cross hatched) [35] is produced and most of the strain is relieved in the vicinity of the interface. The epitaxial layer is closer to perfect crystalline structure when misfit dislocations are present. Recent studies [35, 42] demonstrated that layer-strain energy and the generation of interfacial misfit dislocations at the growth temperature are functions of lattice misfit and layer thickness. Thick layers or a large misfit cause cross-hatched dislocations.

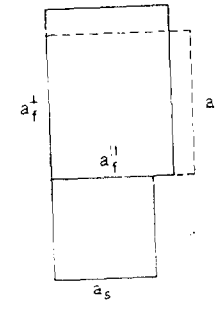

Fig. 16. Deformed and undeformed lattices of an fpitaxial layer on an undeformed substrate.

* 本 論文은 電氣學會誌 第28卷 第4號의 p. 53 論文 28—4—3의 계속임.

In both defects illustrated in Fig. 15, the relative lattice mismatch between the epitaxial layer and substrate can be obtained directly from measurements of the separation angles between the $K_{\alpha 1}$ peaks in X-ray diffraction profiles (so called "rocking curves"). A method is derived below, based on the generalized diagram in Fig. 16, to obtain lattice mismatch and lattice constants.

In Fig. 16, a_s is the lattice constant of the substrate, $a_f^{\perp}$ and $a_f^{\parallel}$ are the strained lattice constants of the epitaxial layer perpendicular and paralled to the substrate surface, and a_f is the lattice constant of the epitaxial layer in the stressfree state. For convenience, these parameters are defined as $\Delta a^{\perp}=a_f^{\perp}-a_s$, $\Delta a^{\parallel}=a_f^{\parallel}-a_s$, and $\Delta a=a_f-a_s$. It has been observed [37, 39, 40] that, in elastic lattice deformation,

$$\frac{\Delta a^{\perp}}{a_s} \gg \frac{(\Delta a^{\parallel})}{a_s} \approx 0 \tag{4.1}$$

If $\Delta\theta_1$ is the separation angle between the $K_{\alpha 1}$ peaks of the substrate and epitaxial layer and if $\Delta\theta_2$ is the same quantity measured after rotating the crystal by 180° around the normal to the substrate surface, the angular difference caused by the variation in lattice spacing $\Delta\theta_B$ is

$$\Delta\theta_B=\frac{\Delta\theta_1+\Delta\theta_2}{2} \tag{4.2}$$

In this measurement, $\Delta\theta_1 \fallingdotseq \Delta\theta_2$ principally because of misorientation of the substrate itself.

The difference in lattice spacing $\Delta a^{\perp}$ was determined through the following equation which was obtained by differentiating Bragg's law:

$$\frac{\Delta a^{\perp}}{a_s}=-\cot\theta_B \times \Delta\theta_B \tag{4.3}$$

where θ_B is the Bragg angle.

From the stress-strain relationship of a cubic crystal, the following equations (see the Appendix for their derivation) are obtained by assuming $\sigma_{xx}=\sigma_{yy}=\sigma^{\parallel}$ and $\sigma_{zz}=\sigma^{\perp}=0$:

$$\sigma^{\parallel}=\varepsilon^{\parallel}\frac{E}{1-\nu_{eff}} \tag{4.4}$$

and

$$\epsilon^{\perp}=\epsilon^{\parallel}\frac{-2\nu_{eff}}{1-\nu_{eff}} \tag{4.5}$$

where σ is the stress and ϵ is the strain, and E and ν_{eff} are Young's modulus and the effective Poisson ratio, respectively. The elastic constants of the layer and the substrate are assumed to be equal [38]. The strains $\epsilon^{\parallel}$ and $\epsilon^{\perp}$ are expressed in terms of $\Delta a^{\perp}/a_s$, $\Delta a^{\parallel}/a_s$, and $\Delta a/a_s$ by

$$\epsilon^{\perp}=\frac{a_f^{\perp}-a_f}{a_f}=\frac{\Delta a^{\perp}-\Delta a}{a_f}\approx\frac{\Delta a^{\perp}}{a_s}-\frac{\Delta a}{a_s} \tag{4.6}$$

and

$$\epsilon^{\parallel}=\frac{a_f^{\parallel}-a_f}{a_f}=\frac{\Delta a^{\parallel}-\Delta a}{a_f}\approx\frac{\Delta a^{\parallel}}{a_s}-\frac{\Delta a}{a_s} \tag{4.7}$$

From the Eqs. (4.1), (4.5), (4.6), and (4.7),

$$\epsilon^{\perp}=\frac{2\nu_{eff}}{1+\nu_{eff}}\frac{\Delta a^{\perp}}{a_s}=\frac{2\nu_{eff}}{1-\nu_{eff}}\frac{\Delta a}{a_s} \tag{4.8}$$

The strain-free relative lattice mismatch can be expressed from the above as

$$\frac{\Delta a}{a_s}=\frac{1-\nu_{eff}}{1+\nu_{eff}}\frac{\Delta a^{\perp}}{a_s} \tag{4.9}$$

The strained and strain-free lattice mismatches have been obtained from Eqs. (4.3) and (4.9), respectively. For misfit dislocations, $(\Delta a/a_s)=-\cot\theta_B\times\Delta\theta_B$ and no effective Poisson ratio is involved.

A. Experiment

The separation angles between the $K_{\alpha 1}$ peaks were precisel measured by an X-ray double-crystal diffractometer. The X-ray target was Cu, and the first crystal was dislocation-free (100) Si. To provide a highly parallel incident beam to the specimen, $CuK_{\alpha 2}$ radiation was cut off with an appropriate slit after the(400) reflection of the first crystal, and $\lambda(CuK_{\alpha 1})=1.54051$ Å. The X-ray penetration depth was estimated to be smaller than 20 μm.

Both (100)-and (111)B-oriented *GaAs* substrates were used to grow epitaxial layers, and measurements were made at room temperature on the (400) and (444) planes, respectively, for the best precision. The Bragg angles were 33.02° and 70.72° for the (400) and(444) reflections of *GaAs* ($a_o=5.6532$Å). The thicknesses of the substrates were approximately 350μm, and the thicknesses of the epitaxial layers were 1 to 4 μm.

1. AlGaAs-GaAs Interface

Addition of *Al* to the *GaAs* melt increases the lattice constant of the *AlGaAs* crystals as com-

pared to *GaAs*. LPE $Al_xGa_{1-x}As$ single layers were grown at 840° to 820°C on both (100)-and (111)B-oriented *GaAs* substrates as the amount of *Al* in the melt was changed (see Chapter III).

The *Al* composition x was independently evaluated by an electron-microprobe analyzer. As discussed in Chapter III, the desired values of x were obtained by changing the weight ratio of *Al* to *Ga* in the melt (no normalization was used). Figure 17 presents typical X-ray diffraction profiles, and the resulting data are summarized in Table 3. Although the theoretical value of full width at half maximum (FWHM) of the rocking curve for a perfectly flat sample is 8.5 seconds, approximately 23 and 143 seconds were observed for (400) and (444) reflections, respectively.

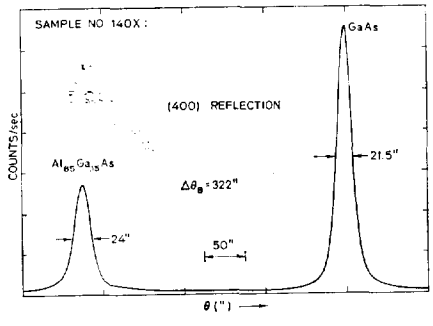

a. (100)-oriented substrate

a. (100)-oriented substrate

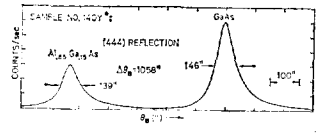

b. (111)B-oriented substrate

Fig. 17. X-Ray Diffraction profiles of LPE $Al_{0.85}Ga_{0.15}As$ layers grown on (100)- and (111)B-oriented *GaAs* substrates.

Figures 18 and 19 plot the measured strained lattice mismatch and the corresponding individual lattice constant as a function of *Al* composition. The results are consistent with the linear behavior predicted by Vegard's law. The best fit

Table 3 Experimental data obtained from lattice-constant measurements of *AlGaAs* single layers

Sample No.	*Al* Composition x	$\Delta a^+/a_s$ ($\times 10^4$)	a_e (Å)
HP1	0.130	3.953	5.6544
HP2	0.213	6.415	5.6551
HP3	0.249	7.310	5.6554
HP4	0.282	8.354	5.6557
HP5	0.308	9.398	5.6560
HP6	0.384	11.114	5.6565
117 J	0.489	14.023	5.6574
118 J	0.627	17.603	5.6584
119 J	0.751	20.512	5.6593
09	0.783	21.556	5.6596
140X	0.851	24.018	5.6603
206	0.846	24.34	5.6604
73	0.899	25.24	5.6607
50	0.939	25.84	5.6609
201B+	0.299	7.375	5.6560
201A+	0.520	12.110	5.6579
152X+	0.738	15.941	5.6595
140Y+	0.851	17.943	5.6603

+These samples are grownon (111)B *GaAs* substrates; all others are on (100) *GaAs* substrates.

for (100)-oriented $Al_xGa_{1-x}As$ epitaxial layers was obtained as $(\Delta a^+/a_s)(Al_xGa_{1-x}As)=(3.54\times 10^{-5})+(28.06\times 10^{-4})x$. Although $\nu_{eff}=0.312$ [42] was adopted for the (100) *GaAs* substrate orientation to determine the strain-free lattice mismatch, $\nu_{eff}=0.190$ was estimated for the (111)B substrate orientation from the ratio of strained lattice mismatch between (100) and (111)B orien-

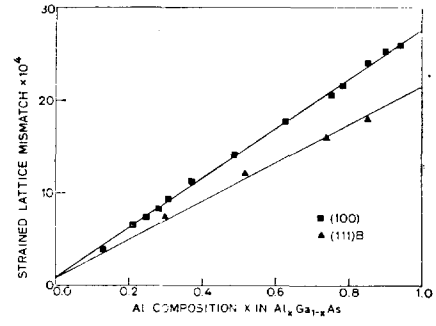

Fig. 18. Strained Lattice Mismatch Between the $Al_xGa_{1-x}As$ epitaxial Layer and the *GaAs* Substrate at 300K as a Function of *Al* Composition x.

tations (see Fig. 18). Although one theoretical estimate [42] indicated $\nu=0.303$ for (111) *GaAs* orientation, no other experimental data are available.

To attain individual lattice constants from the strain-free lattice mismatch (Fig. 19), $a_o(GaAs)=5.6532$Å was assumed. It should be emphasized that, for multiple-layer structures, a double-crystal diffractometer yields only precise lattice mismatch. In the best-fit curve in Fig. 19, $a_o(Al_xGa_{1-x}As)=5.6532+0.0084x$Å which is in good agreement with the result obtained by Estop et al [38].

It should be noted that $Al_xGa_{1-x}As$-$Al_x'Ga_{1-x}'As$ $(x>x')$ double-layer samples have the same separation angles as those in single layers grown from the same melts. In other words, there is no shift in the separation angle caused by the interaction between the epitaxial layer and the substrate.

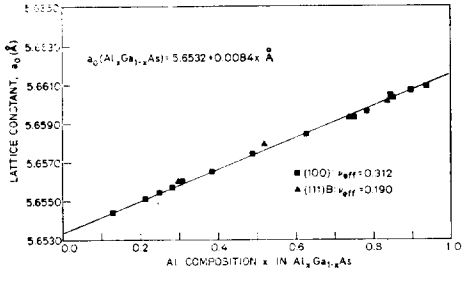

Fig. 19. Strain-Free lattice constant of $Al_xGa_{1-x}As$ single layers on different substrate orientions as a function of *Al* composition x. T=300K.

In conclusion, *AlGaAs* epitaxal layers showed only elastic lattice deformation regardless of *GaAs* substrate orientation. The reason for this is that there is almost a zero-lattice mismatch between the *AlGaAs* layer and the *GaAs* substrate at the growth temperature (see Fig. 22).

2. GaAsSb-GaAs Interface

Just as in the $Al_xGa_{1-x}As$ ternary compound, the addition of *Sb* to *GaAs* causes an increase in the lattice constant. LPE $GaAs_{1-y}Sb_y$ single layers were grown at 840° to 820°C on both (100) and (111)B *GaAs* substrates by changing the amount of *Sb* in the melt (see Chapter III). Although the surface morphology of layers grown on (111)B substrates appeared smooth, the surfaces of most (100) samples displayed cross hatched patterns as the result of misfit dislocations at the interface.

Assuming that the cross-hatched pattern indicates no elastic lattice deformation, ν_{eff} was set equal to 0 for a (100)-oriented layer; in other words, strain-free lattice mismatch can be obtained directly from the separation angles of the X-ray diffraction profiles. In (111) B-oriented *GaAs* substrates, the same effective Poisson ratio ($\nu_{eff}=0.190$) as in *AlGaAs* layers was used, assuming that the elastic constants of the layer and the substrate are equal [38]. The data resulting from these measurements and analyses are summarized in Table. 4. As observed in Chapter III, the data points somewhat scattered because of uncertainty in the *Sb* compositions.

Figure 20 plots the strain-free lattice constants of *GaAsSb* single layers grown on (100) and (111)B *GaAs* substrates as a function of *Sb* composition. Two interesting results are observed. The first is that, when $a_o(GaSb)=6.0959$Å, both (100) and (111)B *GaAsSb* layers deviate slightly from Vegard's law. The other is that lattice-matched $Al_{0.85}Ga_{0.15}As$-$GaAs_{1-y}Sb_y$ double layers can be grown at different *Sb* compositions, depending on substrate orientation; namely, (100) $Al_{0.85}Ga_{0.15}AsGaAs_{0.985}S_{0.015}$ and (111)B $Al_{0.85}Ga_{0.15}As$-$GaAs_{0.976}Sb_{0.024}$ double-heterojunction samples with zero lattice mismatch were grown from melts with a weight ratio of $W_{Sb}/W_{Ga}=0.13$ and a growth temperature of T_G=840 to 820°C. These samples were used in evaluating the measurements of interface recombination velocity as described in Chapter V. Figure 21 is the X-ray diffraction profile of a lattice-matched $Al_{0.85}Ga_{0.15}AsGaAs_{0.976}Sb_{0.024}$ double layer grown on a (111)B *GaAs* substrate. The *AlGaAs* and *GaAsSb* $K_{\alpha 1}$ peaks cannot be resolved because of the extremely close lattice match.

Table 4. Experimental data obtained from lattice-constant measurements of *GaAsSb* single layers

Sample No.	*Sb* Composition *y*	$\Delta a^{\perp}/a_s$ ($\times 10^4$)	$\Delta a/a_s$ ($\times 10^4$)	a_o (Å)
203	0.0069	—	6.04	5.6566
155X	0.0129	—	11.97	5.6600
153	0.0133	—	12.18	5.6601
206	0.0155	—	13.27	5.6607
154X	0.0251	—	22.26	5.6658
122Y+	0.0027	2.33	1.58	5.6541
125X+	0.0056	4.16	2.83	5.6548
123Y+	0.0064	6.15	4.18	5.6556
203+	0.010	8.44	5.74	5.6564
123+	0.0098	8.90	6.05	5.6566
129+	0.0098	11.15	7.58	5.6575
155Y+	0.0181	13.94	9.48	5.6586
161L+	0.0218	16.45	11.19	5.6595
124Y+	0.0166	15.08	10.25	5.6590
202B+	0.0249	19.84	13.49	5.6608
205+	0.0250	18.76	12.76	5.6604
154Y+	0.030	34.02	23.13	5.6663

+These samples are grown on (111)B *GaAs* substrates; all others are on (100) *GaAs* substrates.

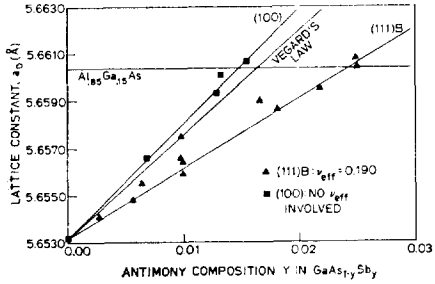

Fig. 20. Strain-Free Lattice Constants of $GaAs_{1+y}Sb_y$ Single Layers on Different Substrate Orientations as a Function of *Sb* Composition. T=300 K.

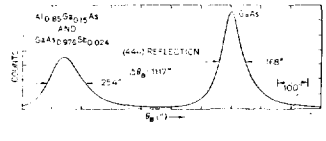

Fig. 21. X-Ray Diffraction Profile of $Al_{0.85}Ga_{0.15}AsGaAs_{0.976}Sb_{0.024}$ Double Layer Grown on (111)B *GaAs* Substrate. T=300 K.

In the above analysis of *GaAsSb* layers, elastic lattice deformation or misfit dislocations were assumed. In reality, both conditions may occur simultaneously [43], which would produce another uncertainty in addition to the microprobe analysis errors.

Althought misfit dislocations in (100) $GaAs_{1-y}Sb_y$ layers are assumed, the results from the double layers (see Table 5) reveal that they could be either elastic lattice deformation (sample D204) or misfit dislocations (sample D203). In addition, lattice constants obtained from the double layers are slightly different than those from single layers, which may be the result, in part, of the uncertainty in ν_{eff}.

Table 5. Experimental data of lattice constant measurements of $Al_{0.85}Ga_{0.15}As$-$GaAs_{1-y}Sb_y$ double layers

Sample No.		*Sb* Composition *y*	$\Delta a^{\perp}/a_s$ ($\times 10^4$)	$\Delta a/a_s$ ($\times 10^4$)	a_o (Å)
D203	*AlGaAs*	0.0069	23.27	12.20	5.6601
	GaAsSb			5.90	5.6565
D203+	*AlGaAs*	0.010	17.86	12.15	5.6601
	GaAsSb		7.12	4.84	5.6559
D204	*AlGaAs*	0.0155	22.02*	11.55	5.6597
	GaAsSb				
D206+	*AlGaAs*	0.025	17.64*	12.00	5.6600
	GaAsSb				
D155Z+	*AlGaAs*	0.0218	18.94*	13.30	5.6607
	GaAsSb				

+Elastic lattice deformation and misfit dislocations were assumed in the *AlGaAs* and *GaAsSb* layers, respectively.
*These separation angles are not resolvable.

B. Discussion

During the analysis of the data, the effects of instrumental broadening (divergence of the beam, focal-spot size, slit width, and spectral width of the X-ray emission wavelength), dislocations and mechanical surface damage on the X-ray diffraction profile were not taken into account. Actually, FWHM increases with increasing curvature and dislocations. Although absolute values of the lattice constants could not be obtained, the precise separation angle between

the two $K_{\alpha 1}$ peaks could be measured. The error in the separation angle caused by the thicknesses of the epitaxial layers was negligible.

The above X-ray measurements in Tables 3 and 4 were made on undoped *AlGaAs* and *GaAsSb* single layers. As a reslut, there may be an additional lattice mismatch on the actual devices caused by the doping of epitaxial layers[36]. Recently, Schiller [41] observed that *AlGaAs* layers grown on (111)A-oriented *GaAs* substrates had slightly lower lattice constants than those on (100) becausehe assumed the same elastic constants (E/1-ν) for both (100) and (111)A orientations.

Figure 22 plots variations of the lattice constants of *GaAs*, $Al_{0.85}Ga_{0.15}As$, and $GsAs_{0.985}Sb_{0.015}$ over a 0 to 1000°C temperature range where the

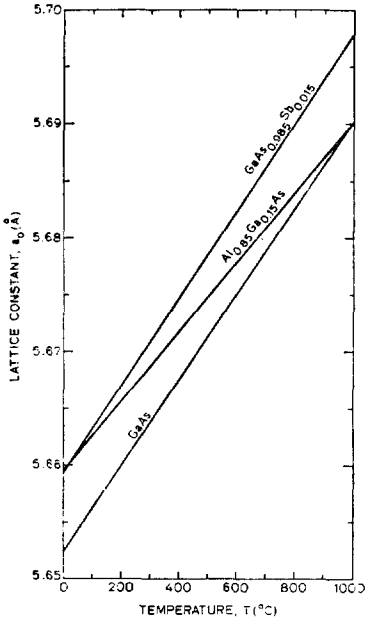

Fig. 22. Variation of Lattice Constants of *GaAs*, $Al_{0.85}Ga_{0.15}As$ and $GaAs_{0.985}Sb_{0.015}$ over the Temperature Range of 0 to 1000°C. It was assumed that $a_o(GaAs)$=5.6532Å, $a_o(AlAs)$=5.6622 Å, and $a_o(GaSb)$=6.0959 Å at 300K. It was also assumed that $\alpha(GaAs)=6.63\times10^{-6}$/°C[44], $\alpha(AlAs)=5.20\times10^{-6}$/°C [45], and $\alpha(GaSb)=6.70\times10^{-6}$/°C [46] over the entire temperature range.

thermal expansion coefficient α of the ternary compounds is assumed to follow a linear relationship between those of the two end binary compounds. As has been discussed, *AlGaAs* epitaxial layers showed elastic lattice deformation only because the lattice mismatch between the *AlGaAs* layer and *GaAs* substrate became almost zero at the growth temperature. The $Al_{0.85}Ga_{0.15}As$-$GaAs_{0.985}Sb_{0.015}$ layers, however, showed large lattice mismatch at the growth temperature although the mismatch became zero at room temperature. The large lattice mismatch between $GaAs_{0.985}Sb_{0.015}$ and *GaAs* at the growth temperature can explain the cross-hatched pattern observed on (100) *GaAsSb* epitaxial layers. No explanation can be made why elastic lattice deofrmation was observed on (111)B *GaAsSb* epitaxial layers. Although the lattice mismatch between the *AlGaAs* and *GaAsSb* epitaxial layers is zero, even the lattice-matched samples display strong strain [35] between the first epitaxial layer and the substrate because of lattice mismatch. Poorer device performance than expected from perfectly lattice-matched samples, therefore, may be observed.

In conclusion, lattice-matched *AlGaAs-GaAsSb* layers can be grown on both (100) and (111)B *GaAs* substrates from the information in Figs. 19 and 20. For example, (100) $Al_{0.85}Ga_{0.15}As$-$GaAs_{0.985}Sb_{0.015}$ and (111)B $Al_{0.85}Ga_{0.15}As$-$GaAs_{0.976}Sb_{0.024}$ double-heterojunction samples with zero lattice mismatch were grown for evaluation from melt swith a weight ratio of W_{Sb}/W_{Ga}=0.13 and a growth temperature of T_G=840~820°C.

5. EFFECTIVE LIFETIME MEASUREMENT

A. EL Time-Decay

Figure 23 is a diagram [6] of the equipment employed to obtain effective lifetime measurements on p-p-n DH diodes. The preparation, I-V characteristics, and EL output of the samples were described in Chapter III.

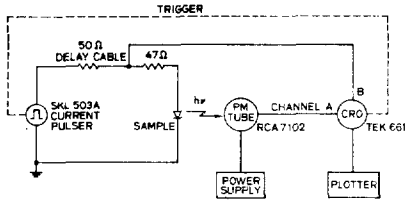

Fig. 23. Diagram of apparatus employed to obtain el time-decay lifetime measurements on DH diodes.

The diodes were excited by 50 nsec square-wave pulses (100pps) from a strip-line pulser (SKL 503A) with a fall time of less than 2 nsec. Minority carrier injection into the (p)*GaAs* (or *GaAs Sb*) layers was low because of the small carrier concentration ($\lesssim 10^{17}/cm^3$) in the (n) *AlGaAs* layers. To detect very weak spontaneous EL output signals, the device was placed directly against an RCA 7102 photomultiplier (PM) tube which had an approximately 2.2 nsec response time.

The detected light pulse was displayed and plotted simultaneously on a sampling oscilloscope (Tektronix 661) having less than a 1 nsec response time and on an X-Y recorder (Beckman 1005 ~02) that produced either linear or log plots of the signals from the oscilloscope output. Figure 24 is a series on linear plots of the detected EL light output pulses from (100)-oriented p-p-n $Al_{0.85}Ga_{0.15}As$-$GaAs_{0.985}Sb_{0.015}$ DH diodes with zero mismatch.

At least three samples for each value of heterojunction spacing d were used to measure the decay times which were determined in the linear portions of the log plots. The results obtained from $Al_{0.85}Ga_{0.15}As$-$GaAs_{1-y}Sb_y$ DH samples are tabulated in Table 6 where, although the measured decay timer were slightly scattered (±0.5 nsec) in each group, the shortest values are listed. A few samples did not reveal a single exponential decay constant (confirmed by the log plots), which may be the result of traps introduced during crystal growth. Bulk lifetime of the minority carriers [6,7,14] was determined from homojunction diodes with thick(~20 μm) p-type

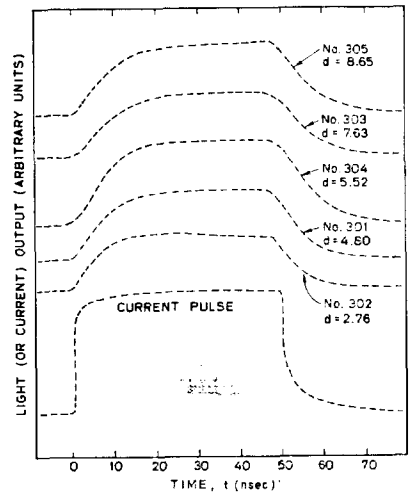

Fig. 24. Linear plots of detected el light output pulses from (100)-oriented $Al_{0.85}Ga_{0.15}As$-$GaAs_{0.985}Sb_{0.015}$ DH diodes. A 50-nsec square wave current pulse was used for excitation. The independent variable is *GaAsSb* thickness d (μm).

GaAsSb layers, using the same technique as described above. In a $GaAs_{0.985}Sb_{0.015}$ Ge layer, τ_o=11 nsec and L_n=1.5μm were measured. These are independent parameters used in the analysis to establish recombination velocity at the $Al_{0.85}Ga_{0.15}As$-$GaAs_{1-y}Sb_y$ interfaces. In the *AlGaAs-GaAs* system, τ=31 nsec and L_n=12μm were used [6] in the evaluation of interface recombination velocities.

Figure 25 plots the normalized minority carrier lifetime vs the normalized heterojunction spacing, with reduced interface recombination velocity as an independent variable. In the *AlGaAs-GaAs* system, a comparison of the experimental data to the theoretical curves (Fig. 25a) reveals that ξ=0.5 (equivalent to $S=2\times10^4$ cm/sec) is the best fit for the $Al_{0.85}Ga_{0.15}As$-*GaAs* DH samples; Ettenberg and Kressel [6] reported that ξ=0.1 (equivalent to $S=4\times10^3$ cm/sec) and ξ=0.2(equivalent to $S=8\times10^3$ cm/sec) for $Al_{0.25}Ga_{0.75}As$-*GaAs* and the $Al_{0.50}$ $Ga_{0.50}As$-*GaAs* DH samples, respectively. It is interesting to note that, rece-

Table 6. Heterojunction device parameters and lifetimes obtained from EL time decay measurements

Composition and Sample No.	Heterojunction Spacing d (μm)	Measured Electron Lifetime τ_{eff} (nsec)
$Al_{0.85}Ga_{0.15}As$-$GaAs$		
81—B	2.54	6.36
82—E	6.27	9.83
85—D	10.08	15.90
$Al_{0.85}Ga_{0.15}As$-$GaAs_{0.985}Sb_{0.015}$		
302	2.76	6.28
301	4.80	5.75
304	5.52	7.30
303	7.63	7.97
305	8.65	8.63
$Al_{0.85}Ga_{0.15}As$-$GaAs_{0.976}Sb_{0.024}$		
302+	1.44	4.20
301+	4.20	3.98
305+	6.48	5.31

+(111)B $GaAs$ substrate orientation.

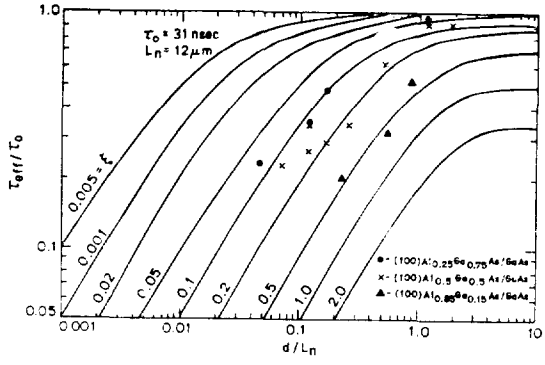

a. $AlGaAs$-$GaAs$ system

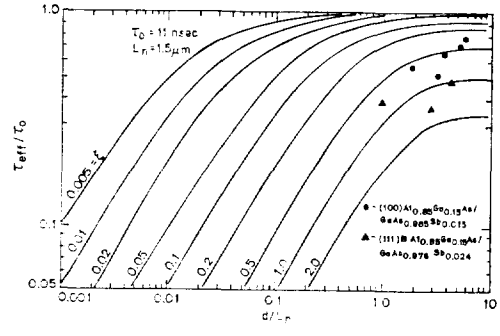

b. $Al_{0.85}Ga_{0.15}As$-$GaAsSb$ system

Fig. 25. Normalized minority carrier lifetime τ_{eff}/τ_0 as a function of normalized heterojunction spacing d/L_n. The independent variable is reduced interface recombination velocity $\xi=SL_n/D_n$.

ntly, $S=3\times10^4$ cm/sec was reported [7] for an $In_{0.5}Ga_{0.5}P$-$GaAs$ interface (0.11 percent mismatch).

In lattice-matched (100)-and (111)B-oriented $Al_{0.85}Ga_{0.15}As$-$GaAs_{1-y}Sb_y$ systems, τ_0=11 nsec and L_n=1.5μm served as the basis for our evaluation of interface recombination velocity. The best fits for the (100)-oriented $Al_{0.85}Ga_{0.15}As$-$GaAs_{0.985}Sb_{0.015}$ and the (111)B-oriented $Al_{0.85}Ga_{0.15}As$-$GaAs_{0.976}Sb_{0.024}$ DH samples were determined to be ξ=0.5 (equivalent to $S=7\times10^3$ cm/sec) and ξ=1.0 (equivalent to $S=1.4\times10^4$ cm/sec), respectively.

B. Optical Phase Shift

1. Curve-Fitting Techniques

Effective minority carrier lifetime can be indirectly determined from optical phase-shift measurements. When the sample is excited by a pulsed laser, the PL output P [14] is

$$P=\frac{C}{(1+j\omega\tau_{eff})+\xi(1+j\omega\tau_{eff})^{1/2}}=C'e^{-j\theta} \quad (5.1)$$

were C, C' are real quantities, ω is the angular frequency of the pulsed laser, and θ is the phase difference (or phase shift). The phase difference θ between the fundamental Fourier component of the scattered laser and PL output of the sample was directly measured by this technique.

To achievea mcre perceptive insight into the curve-fitting technique described above, the following mathematical transformation was made:

$$1+j\omega\tau_{eff}=(1+\omega^2\tau^2_{eff})^{1/2}e^{j\tan^{-1}\omega\tau_{eff}} \quad (5.2)$$

From the denominator of Eq. (5.1), therfore tan θ isdefined as

$$\tan\theta=\frac{\omega\tau_{eff}+\xi(1+\omega^2\tau^2_{eff})^{1/4}\sin(1/2\tan^{-1}\omega\tau_{eff})}{1+\xi(1+\omega^2\tau^2_{eff})^{1/4}\cos(1/2\tan^{-1}\omega\tau_{eff})} \quad (5.3)$$

where, from Eqs. (2.4) and (5.3), tanθ is evaluated as a function of S, d, τ_0, and L_n; in Fig.

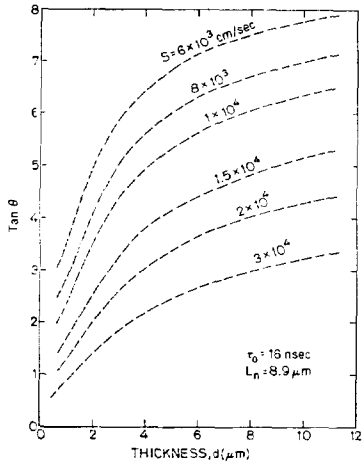

Fig. 26. Determination of the interface recombination velocity by curve fitting of optical phaseshift data.

26, τ_o=16 nsec and L_n=8.9μm are the fixed variables. As demonstrated in Chapter II, for given values of τ_o and L_n, the interface recombination velocity S is determined by curve fitting from the measured values of d and θ. It can be seen in Fig. 26, that tanθ decreases with decreasing d and increasing S; it also increases with increasing τ_o. when τ_o is varied from 13 to 28 nsec, there is little difference in tanθ when $d<10\mu$m which indicates that τ_o is not critical at certain ranges when determining S. In addition, when τ_o is smaller than 1 nsec, the curves for different values of S are very closely located. As a result, this type of analysis is inadequate for the evaluation of interface recombination velocity. Similar curve-fitting techniques have been used by Hopkins [9].

2. Phase-Shift Measurement

Figure 27 is a plot of the intensity modulation of a Kr-ion laser beam (Coherent Radiation, Inc., 500K) obtained by a mode-locker (Coherent Radiation, Inc., 465) and included is a diagram of the equipment employed in optical phase-shift measurements. The repetition frequency of the pulsed laser beam was $f\approx$114MHz (Fig. 27a), and the

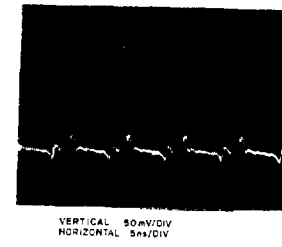

a. Intensity modulation of a Kr-ion laser beam

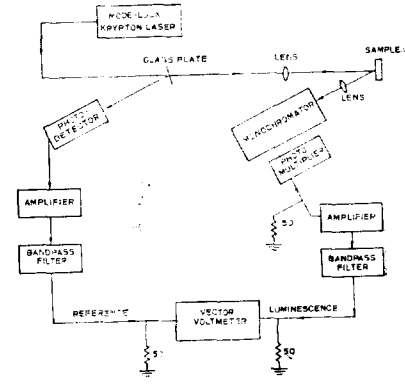

b. Equipment

Fig. 27. Optical phase-shift measurements.

average power was P_{avg}=50mW. The sample was excited by the 6471Å laser line. The penetration depth in *GaAs* and *GaAsSb* layers was ~1/4 μm. A small part of the laser beam was detected by a Si avalanche photodetector after it had been separated from the main beam by asplitter (glass plate) and amplified by an HP 461A. After passing through a bandpass filter, it was used as a reference signal (channel A) of the vector voltmeter (HP 8405A). The PL output of the sample was detected by a photomultiplier (RCA C31024A or RCA 7102) after passing through a grating spectrometer (SPEX 1672 Double Mate) with a 5Å resolution (0.25mm slit width) and was then directed to the signal channel of the vector voltmeter through an amplifier (HP 462 A) and a bandpass filter. The difference in phase between the photoexcitation and PL output

of the sample ismeasured by the vector voltmeter which can also measure absolute signal amplitudes on both channels. The phase difference between the scattered excitation signal and the reference-channel signal establishes a"zero" phase difference. The phase shifts were measured at the PL peaks that had been produced from band to-band transitions.

In this study, the phase shifts (or radiative lifetimes) were obtained at a sufficiently low excitation level for the hole concentration to equal approximately its equilibrium value so as to ensure that the bulk lifetime is constant. Such measurements were made at room temperature, and the results (namely, $\tan\theta$) are listed in Table 7. It was also observed that the short wavelength PL output ($>E_g$) had smaller phase shifts (shorter radiative lifetimes) and that the long wavelength PL output ($<E_g$)had larger phase shifts (longer radiative lifetimes.).

Figure 28 plots $\tan\theta$ vs d from the data in Table 7. In the *AlGaAs-GaAs* system, τ_o=16 nsec was measured by the same optical phase shift technique. Curve fitting the experimental data with the theoretical curves (see Fig. 28a) indicates that $S=3\times10^4$cm/sec and $L_n=8.9\mu$m are the best fits at an $Al_{0.85}Ga_{0.15}As$-$GaAs$ interface. Although a differnt vealue of τ_o was used in the previous curve-fitting analyses of the EL time-decay data, the two measuring techniques (EL time decay and optical phase shift) produce similar results. The different values of τ_o may stem from the fact that EL is an electrical injection mode and PL is an optical injection mode; however, τ_o is not critical at certain ranges when determining S (see Section B. 1). The effective lifetime of sample DH-35 was measured at both 300 and 77K, and it was observed that its lifetime increased from 3.6 nsec at 300K to 23.4 nsec at 77K.

In lattice-matched (100)-and (111)B-oriented $Al_{0.85}Ga_{0.15}As$-$GaAs_{1-y}Sb_y$ systems (Fig. 28b), τ_o= 14 nsec was measured. The best fits are $S=6\times10^3$ and 2×10^4cm/sec with $Ln=3.74\mu$m at the (100)-oriented $Al_{0.85}Ga_{0.15}As$-$GaAs_{0.985}Sb_{0.015}$ and (111)B oriented $Al_{0.85}Ga_{0.15}As$-$GaAs_{0.976}Sb_{0.024}$ interfaces, respectively.

Table 7. Heterojunction device parameters for optical phase shift

Composition and Sample No.	Heterojunction Spacing $d(\mu m)$	Phase-Shift $\tan\theta$
$Al_{0.85}Ga_{0.15}As$-$GaAs$		
39	3.2	1.78 to 2.18
42	5.0	2.00 to 2.78
37	5.7	2.37 to 2.92
35	6.6	2.20 to 3.06
40	8.0	2.79 to 3.33
38	9.0	2.69 to 3.19
$Al_{0.85}Ga_{0.15}As$-$GaAs_{0.985}Sb_{0.015}$		
210	1.12	1.73 to 1.80
213	3.84	4.33 to 4.70
207	5.52	5.67 to 6.31
212	6.00	4.92 to 5.14
211	6.96	5.14 to 5.67
208	9.61	5.14 to 5.67
209	11.89	5.67 to 6.31
$Al_{0.85}Ga_{0.15}As$-$GaAs_{0.983}Sb_{0.017}$		
135B+	2.16	2.36 to 2.75
133B+	2.28	3.27 to 3.73
135A+	2.35	3.49 to 4.01
134A+	3.00	3.73 to 4.33
133A+	3.60	3.73 to 4.70
$Al_{0.85}Ga_{0.15}As$-$GaAs_{0.976}Sb_{0.024}$		
213+	2.40	2.05 to 2.14
207+	2.74	1.33 to 1.38
211+	4.80	2.36 to 2.48
208+	5.88	2.25 to 2.36
209+	7.80	2.48 to 2.61

+(111)B *GaAs* substrate orientation.

C. Discussion

Figure 29 summarizes the measured values of interface recombination velocity as a function of strain-free lattice mismatch at room temperature. The ● indicates the (100)-oriented $Al_xGa_{1-x}As$-$GaAs$ interface system, and ▲ and ■ denote (100)-and (111)B-oriented $Al_{0.85}Ga_{0.15}As$-$GaAs_{1-y}Sb_y$ interface systems, respectively. In addition,

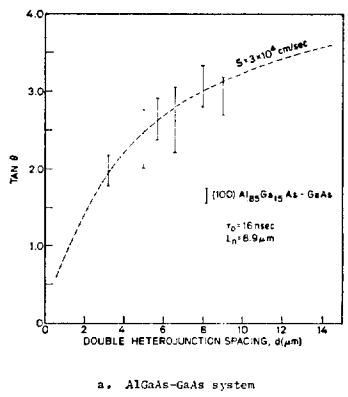

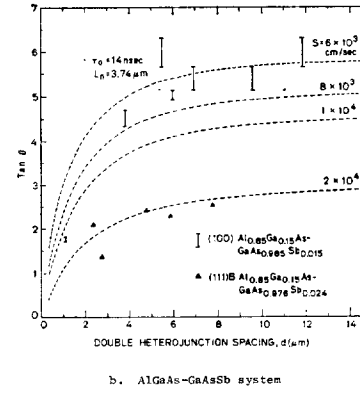

a. *AlGaAs-GaAs* system　　b. *AlGaAs-GaAsSb* system

Fig. 28. Determination of Interface recombination velocity by curve fitting of the optical phase shift data. data taken at 300K.

○ desgnates optical phase-shift measuremients, whereas the remaining points specify EL time-decay measurements. In the *AlGaAs-GaAs* system, the points at 0.038 percent (x=0.25) and 0.075 percent (x=0.50) mismatch are those reported by Ettenberg [6] of RCA, and the ones at 0.126 percent (x=0.85) mismatch are the results obtained from this analysis. Note an exponential relationship between interface recombination velocity and lattice mismatch.

The addition of 1.5 percent *Sb* to(100)-oriented *GaAs* produces a near-zero mismatch in $Al_{0.85}Ga_{0.15}As$ and lowers the interface recombination velocity from (2 to 3)×10⁴ cm/sec (y=0) to (6 to 7)×10³cm/sec. Although this value is slightly higher than expected from the linear relationship in the semilog plot, solar cells made from such a combination of materials should have an excellent spctral response at short wavelengths resulting from the large band gap of the $Al_{0.85}Ga_{0.15}As$ window material (E_g=2.05eV) and at long wavelengths because of the addition of *Sb* to the *GaAs* active layer. Theoretical studies [20, 47] indicate that, when the interface recombination velocity becomes less than 10⁴cm/sec, further reduction in S poes not improve the solar-cell spectral response. The lattice-matched *AlGaAs-GaAsSb* solar cells developed in this research, therefore, are nearly ideal in this respect.

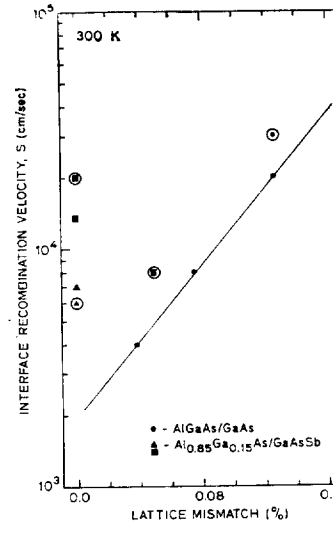

Fig. 29. Interface recombination velocity vs lattice mismatch at 300K In $Al_xGa_{1-x}As$-$GaAs$ and $Al_{0.85}Ga_{0.15}As$-$GaAs_{1-y}Sb_y$ double heterojunctions. The ●, ▲, ■ are from EL time-decay techniques, and ◉, (▲), (■), are from optical phase-shift techniques.

Similar measurements on a lattice-matched (111)B-oriented $Al_{0.85}Ga_{0.15}As$-$GaAs_{0.976}Sb_{0.024}$ interface resulted in S=(1.4 to 2)×10⁴ cm/sec, and S=9×10³cm/sec was obtained at a (111)B-oriented $Al_{0.85}Ga_{0.15}As$-$GaAs_{0.983}Sb_{0.017}$ interface(~0.048

percent mismatch at 300K). Both samples revealed elastic lattice deformation without misfit dislocations.

Ettenberg [8] obtained $S=2.5\times10^4$ and 3×10^4 cm/sec at $In_{0.503}Ga_{0.497}P$-$GaAs$ (~0.14 percent mismatch at 300K)and $In_{0.491}Ga_{0.509}P$-$GaAs$(~0.048 percent mismatch at 300K) heterojunction interfaces, respectively. Both samples displayed only elastic lattice deformation. The $In_{0.491}Ga_{0.509}P$-$GaAs$ interface had approximately the same recombination velocity as that of our $Al_{0.85}Ga_{0.15}As$-$GaAs$ interface although the former had a much smaller attlice mismatch at 300K. Ettenberg concluded that, When the lattice constant of epitaxial layers was larger than the underlying substrate, the interface recombination velocity varies linearly as a function of growth-temperature lattice mismatch resulting in misfit dislocations; however, there were no misfit dislocations in the above $InGaP$-$GaAs$ samples.

6. CONCLUSIONS AND RECOMMENDATIONS

A. Conclusions

The interface recombination velocity as a function of lattice mismatch at $Al_xGa_{1-x}As$-$GaAs$ (or $GaAs_{1-y}Sb_y$) heterojundtion interfaces was investigated. p-p-p and p-p-n DH samples were prepared on (100)-and (111)B-oriented boat-grown (n)$GaAs$: Te substrates, using a horizontal sliding boat LPE growth sytems. The values of x and y were controlled by adding known amounts of Al or Sb to As-saturated Ga melts. Auger analyses in addition to Al or Sb concentration microprobe line profiles and PL spectra revealed that the DH samples had nearly abrupt heterojunctions and that ther was no perceptible cross diffusion of Al or Sb at the interfaces.

A method was developed to determine the lattice mismatch and the lattice constants in mixed single crystals. When hetercepitaxial layers were grown, either elastic lattice deformation or misfit dislocations were observed because of the differences in the lattice constants and thermal expansion coefficients. An effective Poisson ratio was applied to the elastic lattice-defromation condition to detect the strain-free lattice mismatch from the strained lattice mismatch; in misfit dislocations, the strain-free lattice mismatch was obtained directly from X-ray diffraction profiles rather than from the Poisson ratio. From precise measurements of $AlGaAs$ single layers grown on $GaAs$ substrates, $\nu_{eff}=0.312$ and 0.190 were observed in (100)-and (111)B-oriented $AlGaAs$ layers, respectively. No ν_{eff} was involved in the (100)-oriented $GaAsSb$ layers although $\nu_{eff}=0.190$ was chosen for the (111)B-oriented $GaAsSb$ layers.

Assuming that $a_o(GaAs)=5.6532$Å resulted in $a_o(Al_xGa_{1-x}As)=5.6532+0.0084x$ Å which is in good agreement wiht Vegard's law. Lattice-matched $Al_{0.85}Ga_{0.15}As$-$GaAs_{1-y}Sb_y$ layers were grown on both (100)-and (111)B-oriented $GaAs$ substrates at a ratio of $W_{Sb}/W_{Ga}=0.13$ and a temperature of 840 to 820°C although the corresponding Sb compositions were different ($y=0.015$ and 0.024) because of the dependence of the Sb distribution coefficient on substrate orientation. When $a_o(GaSb)=6.0959$Å was assumed at 300K,both(100)-and (111)B-oriented $GaAsSb$ layers deviated only slightly from Vegard's law.

Interface recombination velocity in the $Al_{0.85}Ga_{0.15}As$-$GaAs_{1-y}Sb_y$ system was determined from the dependence of the effective minority carrier lifetime on double-heterojunction spacing, using both optical phase shift and EL time decay, and good agreement between these recombination velocities was obtained by the two techniques. The addition of 1.5 percent Sb to (100)-oriented $GaAs$ produces a near-zero mismatch with $Al_{0.85}Ga_{0.15}As$ and lowers the velocity from(2to 3)$\times10^4$ ($y=0$) to (6 to 7)$\times10^3$cm/sec. Lattice-matched (100)-oriented $Al_{0.85}Ga_{0.15}As$-$GaAs_{0.985}Sb_{0.015}$ solar cells have sufficiently low values of S to make them nearly ideal devices. They should have an excellent spectral response to photons with energies over the full range from 1.4 to 2.6eV.

B. Recommendation

The recombination velocities at $Al_{0.85}Ga_{0.15}As$

$GaAs_{1-y}Sb_y$ heterojunction interfaces were measured only at room temperature. An exponential relationship between interface recombination velocity and lattice mismatch was observed in the *AlGaAs-GaAs* system; however, these velocities deviated at $Al_{0.85}Ga_{0.15}As$-$GaAs_{1-y}Sb_y$ interface. As a result, termal expansion coefficient measurements of these ternary materials should be conducted over the range from room to growth temperatures so as to determine the general relationship between interface recombination velocity and lattice mismatch in systems based on different materials. The analysis should include a quantitative evaluation of the contributions of misfit dislocations and elastic strain to recombination velocity. The measurements should also extend to *AlGaAsP-GaAs* interfaces. The information obtained from all of these measurements can then be used to optimize the performance of heterojunction solar cells and other devices such as light-emitting diodes and laser diodes.

This investigation has demonstrated that the recombination velocity at a $Al_{0.85}Ga_{0.15}As$-$GaAs_{0.985}Sb_{0.015}$ attice-matched heterojunction is sufficiently small for maximum solar-cell collection efficiency. This result should be tested by constructing working models of (p)$Al_{0.85}Ga_{0.15}As$-(p)$GaAs_{0.985}Sb_{0.015}$-(n)*GaAs* solar-cell structures. The spectral response, short-circuit current, fill factor, and conversion efficiency should be examined under terrestrial sunlight conditions and compared to conventional *AlGaAs-GaAs* solar cells.

Appendix

Elastic Deformation of Cubic Lattice and Related Elastic Constants [48]

Two-Dimensional Case: $\sigma^{\perp}=0$

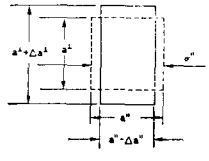

Definition

$E=\sigma^{\parallel}/\epsilon^{\parallel}$

$\nu=-\epsilon^{\perp}/\epsilon^{\parallel}$

then,

$\epsilon^{\parallel}=(1/E)\sigma^{\parallel}$

$\epsilon^{\perp}=(-\nu/E)\sigma^{\parallel}$

Three-Dimensional Case: $\sigma_{zz}=0$ and $\sigma_{xx}=\sigma_{yy}=\sigma$

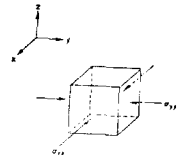

$$\epsilon_{xx}=\epsilon_{yy}$$
$$=\epsilon^{\parallel}+\epsilon^{\perp}$$
$$=(1-\nu/E)\sigma^{\parallel}$$
$$\epsilon_{zz}=2\epsilon^{\perp}$$
$$=(-2\nu/E)\sigma^{\parallel}$$
$$=(-2\nu/1-\nu)\epsilon_{xx}$$

REFERENCES

1. J.J. Loferski, 25th Annual Proc. Power Sources Conf. (May 1972), pp.1~4.
2. H. Fischer, *Festkörperprobleme XIV Advances in Solid State Physics*, Edited by H.J. Queisser, Stuttgart (Pergamon-Vieweg, 1974), pp. 153~182.
3. L.W. James and R.L. Moon, Appl. Phys. Lett. **26**, 476 (1975).
4. H.C. Casey, Jr. and F.A. Trumbore, Mat. Sci. and Eng. **6**, 69 (1970).
5. A. Many, Y. Goldstein, and N.B. Grover, *Semiconductor Surfaces* (North-Holland, Amsterdam, 1965).
6. M. Ettenberg and H. Kressel, J. Appl. Phys. **47**, 1538 (1976).
7. M. Ettenberg, C.J. Nuese, and G. H. Olsen, J. Appl. Phys. **48**, 1288(1977)
8. M. Ettenberg and G.H. Olsen, J. Appl. Phys. **48**, 4275 (1977).
9. R.H. Hopkins, J.R. Davis, P. Rai-Choudhusy, P.D. Blais, and J.R. McCormick, "Silicon Materials Task of the Low Cost Solar Array Project (Part 2)," Secontd Quarterly Report, 1 January-31 March 1976, Westinghouse Research Laboratories, p. 43.
10. E.M. Pell, Phys. Rev. **90**, 278 (1953).
11. R.H. Dean and C. J. Nuese, IEEE Trans. **ED 18**, 151 (1971).
12. G.A. Acket, W. Nijman, R.P. Tijburg, and P.J. de Waard, *GaAs and Related Compounds*, Inst. Phys. Conf. Ser. No. **24**, 181(1975).
13. D.L. Keune, N. Holonyak, Jr., R.D.Burnham, D.R. Scifres, and H. R. Zwicker, J. Appl. Phys. **42**, 2048 (1971).

14. G.A. Acket, W. Nijman, and H.'t Lam, J. Appl. Phys. **45**, 3033 (1974).
15. D.T. Cheung, "Properties of III-V Compound Heterojunctions Prepared by Liquid Phase Epitaxial Techniques," Ph.D. dissertation, SEL-75-013, Stanford University, Stanford, Calif. (1975), p.12.
16. M.B. Panish, J. Appl. Phys. **44**, 2659 (1978).
17. J. Vilms and J.P. Garrett, Solid State Electronics **15**, 443 (1972).
18. A.J. Spring Thorpe, F.D.King, and A.Becke, J. Elect. Mat. 4, 101 (1975).
19. K.K. Shih and G.D. Pettit, J. Elect. Mat. **3**, 391 (1974).
20. L.C.-C. Shen, "Preparation and Properties of Grown Junction *GaAs* Solar Cells," Ph.D. dissertation,SEL-76-020, Stanford University, Stanford, Calif. (1976), p.40.
21. T.Y. Wu and G.L. Pearson, J. Phys. Chem. Solids 33, 409 (1972).
22. G.A. Antypas, J. Electrochem. Soc. **117**, 1393 (1970).
23. M. Kurihara, T. Moriizumi, and K. Takahashi, Solid State Electronics **16**, 763 (1973).
24. M. Ettenberg and H.F. Lockwood, *GaAs and Related Compounds*, Inst. Phys. Conf. Ser. No. **24**, 102(1975).
25. D. Huber and W. Gramman, *GaAs and Related Compounds*, Inst. Phys. Conf. Ser. No. **24**, 223 (1975).
26. M. Ettenberg, C.J. Nuese, J.R. Appert, J.J. Gannon, and R.E. Enstrom, J. Elect. Mat. **4**, 37 (1975).
27. B. Schwartz, J.C.. Dyment, and S.E. Haszko, *GaAs and Related Compoundds*, Inst. Phys. Conf. Ser. No. **17**, 187 (1973).
28. R.A. Logan and F.K.Reinhart, J.Appl. Phys. **44**, 4172 (1973).
29. F.E. Rosztoczy, F. Ermanis, I. Hayashi, and B. Schwartz, J. Appl. Phys. **41**, 264 (1970).
30. A.G. Milnes, *Deep Impurities in Semiconductors*, Wiley-Interscience (1973), p.47.
31. C.M. Garner, Y.D. Shen, J.S. Kim, G.L. Pearson, W.E. Spicer, J.S. Harris, and D.D. Edwall, J. Appl. Phys. **48**, 3147 (1977).
32. C.M. Garner, Y.D. Shen, J.S. Kim, G.L. Pearson, W.E. Spicer, J.S. Harris, D.D. Edwall, and R. Sahai, J. Vac. Sci. Technol. **14**, 985 (1977).
33. L. Jastrzebski, J. Lagowski, and H.C. Gatos, Appl. Phys. Lett. **27**, 537 (1975).
34. A.M. Sekela, D.L. Feucht, and A.G. Miles, *GaAs and Related Compounds*, Inst. Phys. Conf. Ser. No.**24**, 245 (1975).
35. G.A. Rozgonyi, P.M. Petroff, and M.B. Panish' J. Growth **27**, 106 (1974).
36. S. Kishino, M. Ogirima, T. Kajimura, and K. Kurata, J.Cryst. Growth **24/25**, 266(1974).
37. S. Isomae, S. Kishino, and M. Takahashi, J. Cryst. Growth **23**, 253 (1974).
38. E. Estop, A. Izrael, and M. Sauvage, Acta Cryst. **A32**, 627 (1976).
39. T. Hattanda and A. Takeda, Japan J. Appl. Phys. **12**, 1104 (1973).
40. K. Ishida, J. Matsui, T. Kamejima, and L. Sakuma, Phys. Stat. Sol. **(a)31**, 225 (1975).
41. C. Schiller, *GaAs* and Related Compounds, Inst. Phys. Conf. Ser. No. **33a**, 25 (1977).
42. W.A. Brantley, J. Appl. Phys. 44,534 (1973).
43. H. Nagai, J. Appl. Phys. **45**, 3789 (1974).
44. I. Kudman and R.J. Paff, J. Appl. Phys. **43**, 3760 (1972).
45. M. Ettenberg and R.J. Paff, J. Appl. Phys. **41**, 3926 (1970).
46. J.C. Woolley, J. Electrochem. Soc. **112**, 461 (1965).
47. J.M. Woodall and H.J. Hovel, Appl. Phys. Lett. **21**, 379 (1972).
48. H.W. Hayden, W.G. Moffatt, and J. Wulff, *The Structure and Properties of Materials*, Vol. III (Mechanical Behavior) (John Wiley & Sons, Inc., N.Y., 1965), p.24.